Bridging Large–Signal and Small–Signal Responses of Hafnium–Based Ferroelectric Tunnel Junctions

M. Massarotto[1], M. Segatto[1], F. Driussi[1], A. Affanni [1], S. Lancaster [2], S. Slesazeck [2], T. Mikolajick [2,3], D. Esseni[1]

[1]DPIA, Università degli Studi di Udine, Via delle Scienze 206, Udine, Italy

[2]NaMLab gGmbH, Nöthnitzer Str. 64a, 01187 Dresden, Germany

[3]IHM TU Dresden, Nöthnitzer Str. 64, 01187 Dresden, Germany

Abstract: Ferroelectric Tunnel Junctions (FTJs) are interesting energy–efficient devices for many applications, nevertheless, their operation is not completely assessed yet and a full understanding of experiments is required. Notably, large– and small–signal characterizations of FTJs have often led to discrepancies in the interpretation of the results. Through an in–house–developed experimental setup and modeling, novel measurements are performed and interpreted, providing, for the first time to our knowledge, a bridge between the quasi–static and AC responses of FTJs.

Lead author: Marco Massarotto

DPIA, Università degli Studi di Udine

via delle Scienze, 206

33100, Udine, Italy

FAX: +39-0432558251

e.mail: massarotto.marco001@spes.uniud.it

Authors preference: ORAL PRESENTATION

Bridging Large–Signal and Small–Signal Responses of Hafnium–Based Ferroelectric Tunnel Junctions

M. Massarotto[1], M. Segatto[1], F. Driussi[1], A. Affanni [1], S. Lancaster [2], S. Slesazeck [2], T. Mikolajick [2,3], D. Esseni[1]

[1]DPIA, University of Udine, Italy [2]NaMLab gGmbH, Dresden, Germany [3]IHM TU Dresden, Germany

Introduction. HfO_2–based Ferroelectric Tunnel Junctions (FTJs) in a Metal–Ferroelectric–Dielectric–Metal (MFDM) structure (Fig.1) are investigated as energy–efficient synapses for neuromorphic computing [1, 2]. To optimize the FTJs, a thorough understanding of their operation is required to assess the trade–offs between the stored polarization, charge trapping and the read current [3]. But, standard measurement techniques appear insufficient to fully understand the FTJ operation; e.g. the measured small–signal (AC) capacitance C_{AC} is difficult to be compared to quasi–static characteristics of FTJs [4]. In fact, ferroelectric (FE) spontaneous polarization largely contributes to the quasi–static response, while it is much less visible in the measured C_{AC}, leading to some controversy in the interpretation of experiments [5, 6, 7].

In [8] we developed an experimental setup (Figs.1, 2) for FTJ quasi–static characterization (large signals, LS, at low frequency f). We here validate the setup also for AC analysis (at medium/high f) and propose original procedures that provide a bridge between the LS and AC experiments, which are also interpreted through physics–based modeling [3].

Devices and operation. MFDM stacks are fabricated by depositing via ALD 10 nm $Hf_{0.5}Zr_{0.5}O_2$ (HZO) and 2 nm Al_2O_3 on bottom W (30 nm)/TiN (10 nm) electrodes (Fig.1). Top contact is 10 nm TiN, deposited by reactive sputtering. Capacitors are defined by depositing Ti (10 nm)/Pt (25 nm) through a shadow mask, used for etching of the TiN layer. FE polarization P is switched by the applied voltage V_{IN} (Fig.1), which leads to different band profiles and read currents for each polarization state [3]. Polarization state is studied by measuring the switching current I_{FTJ} during V_{IN} pulse.

Experiments and simulations. During the V_{IN} application, a virtual–grounded I–V converter connected to an oscilloscope measures I_{FTJ} (Figs.1, 2). The application of triangular V_{IN} pulses allows us to distinguish I_{FTJ} peaks due to P switching from the essentially V_{IN}–independent I_{FTJ} due to the dielectric response [8]. Integration of the measured I_{FTJ} allows calculating the switching charge Q_{FTJ}, which is used to obtain the hysteretic P–V_{IN} curve of FTJs (Fig.3a).

The developed setup is also used for AC analysis: we issue to the FTJ the triangular LS pulse reaching a voltage V_0, and then superimpose to the bias V_0 a small–signal wave (sinusoidal or triangular) as shown in Fig.4. The setup allows us to test the AC response in LS measurement conditions used to obtain the P–V_{IN} curve. Fig.5 shows the time evolution of applied V_{IN} (a) and the measured I_{FTJ} (b,c). For V_0 close to the FTJ coercive voltages ($\pm V_c$, Fig.4), in the first pulse periods we see large I_{FTJ} peaks due to irreversible switching (Fig.5b), which are not observed for V_0 far from $\pm V_c$ (Fig.5c). Peaks in the Probability Density Function of I_{FTJ} in Fig.5(d,e) are used to extract the I_{FTJ} pulse amplitude, whose value is divided by the V_{IN} slew rate to obtain the AC differential capacitance (C_{AC}, Fig.6, symbols). These C_{AC} values have been verified by comparison with those measured through an LCR meter (Fig.7). The good agreement in Fig.6 confirms the setup validity also for AC analysis. Peaks in C–V curves are ascribed to the FE domain dynamics [4].

Figure 6 highlights the small contribution of irreversible switching to the measured C_{AC} as compared to the effective LS capacitance C_{LS} calculated from the LS response (Fig.3b) [4]. In fact, the C_{LS} peak (C_{SW}) is much larger in Fig.3b than in Fig.6, while the baseline (C_{LIN}) of the two curves is the same. Such behaviour has been observed routinely in the literature [4, 5, 6]. To study this point, we simultaneously probe the AC and LS responses by measuring I_{FTJ} during the application of a waveform (Fig.8a) consisting of an LS triangular pulse with a superimposed small sinusoidal wave with frequency f_{AC}. Fig.8b shows the measured I_{FTJ}, clearly featuring sinusoidal fluctuations on top of the I_{FTJ} contribution due to the LS triangular sweep (dashed orange). Proper numerical filtering allows separating the current component I_{AC} due to the AC sinusoidal signal alone from the LS response. We used I_{AC} to calculate C_{AC}=$I_{AC} \times (dV/dt)^{-1}$ (Fig.9), whose envelope has the same qualitative features as the capacitance measured with the LCR (Fig.7) and as C_{LS} in Fig.3b. In fact, two peaks emerge from the baseline C_{LIN} in correspondence of $\pm V_c$, that we will further analyse below.

To monitor the irreversible switching contribution in these measurements, in Fig.10 we show the $\Delta C = C_{SW} - C_{LIN}$ further divided by C_{LIN} (see Fig.9) as a function of the frequency of the LS triangular pulse and for a fixed f_{AC}=100 kHz. Peak amplitudes lie between a minimum set by the LCR meter experiments in Fig.7 and a maximum set by C_{LS} in Fig.3b. ΔC=(C_{SW}−C_{LIN}) depends on the LS frequency: at low frequency, C_{SW} is close to the results of the LCR meter experiments, while for the largest LS frequency C_{SW} approaches the results in Fig.3b. Hence, this experiment provides a bridge between capacitance/charge values measured in FTJs undergoing either an LS characterization or AC analysis. In Fig.11 we extracted ΔC also as a function f_{AC}, namely the frequency of the AC stimulus, at fixed frequencies of the LS sweep. ΔC increases while decreasing f_{AC}, hence the irreversible switching contribution to C_{SW} grows at low AC frequencies. The large f_{AC} dependence of ΔC in Fig.11 is not visible in LCR meter experiments (yellow line).

In order to investigate the experiments, we used the calibrated, physics–based model presented in [9]. Landau, Ginzburg, Devonshire (LGD) theory is used to model the FTJs, also including trapping at the HZO–Al_2O_3 interface [10]. The simulated LS curve agrees well with experiments (Fig.3). We also simulated the FTJ response to the V_{IN} wave in Fig.8a and then calculated the resulting $\Delta C/C_{LIN}$ thus emulating the experiments. Simulations (Figs.10, 11, green) show a good agreement with the trends in the measurements, confirming the C_{SW} dependence on the LS speed and f_{AC}.

Conclusion. An in-house setup and new experiments are used to explain the FTJ behaviour across the entire measurement range from LS to AC analysis, for the first time. Contribution of FE switching to C_{AC} is small in LCR experiments, while it grows if the underlying bias changes over time. A fast LS sweep may destabilize the FE configuration, allowing the polarization switching to respond to the AC signal. Instead, a stable DC bias stabilizes the FE, reducing the AC response. C_{AC} peak dependence on f_{AC} may be explained by time constants related to polarization–trapping interplay.

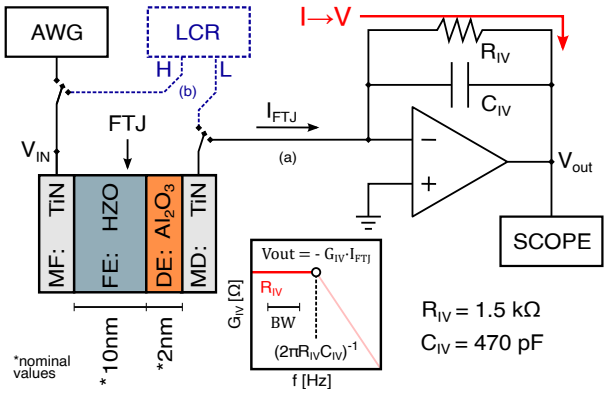

Figure 1: Sketch of the MFDM FTJs and of the experimental setup used in this work. (a) Here, the virtual–grounded amplifier is used as an I→V converter to probe the switching current I_{FTJ}, but it can also operate as an integrator to directly measure the ferroelectric switching charge Q_{FTJ} [8]. The Arbitrary Waveform Generator (AWG) drives the FTJ and V_{OUT} is monitored through an oscilloscope. The transfer function of the converter is also sketched. (b) The setup includes also an LCR meter for standard small–signal characterizations.

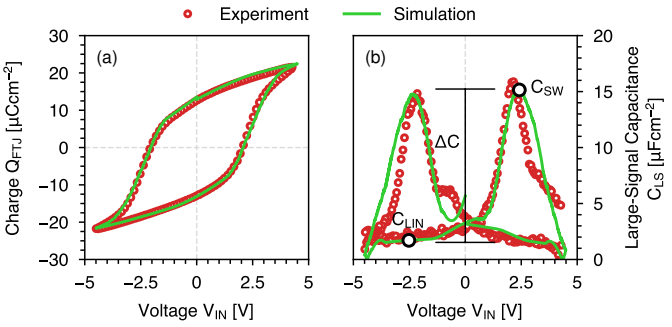

Figure 3: (a) Measured (symbols) and simulated (line) switching charge Q_{FTJ} versus V_{IN} curves. Experimental Q_{FTJ} is obtained by applying triangular V_{IN} pulses and by integrating the measured switching current I_{FTJ}. Q_{FTJ} is typically interpreted as switched polarization P. (b) Effective large–signal capacitance (C_{LS}) versus V_{IN} curve, extracted by dividing I_{FTJ} by the slope of the voltage ramp, namely as $C_{LS} = I_{FTJ}/(dV_{IN}/dt)$.

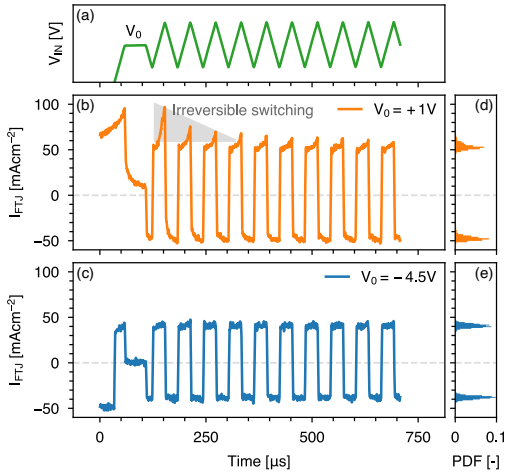

Figure 5: AC analysis with triangular pulses (f_{AC}=17 kHz). Time evolution of V_{IN} (a) and of I_{FTJ} measured for two V_0 values respectively close to the coercive voltage V_c (b) and far from V_c (c) of the P–V curve (Fig.4). Irreversible switching (shaded area) is observed only in the very first AC periods and when V_0 is close to the FTJ coercive voltages. When V_0 is far from $\pm V_c$, the I_{FTJ} amplitude is constant for all pulses. (d, e) Probability Density Functions of I_{FTJ} used to extract the I_{FTJ} amplitude for capacitance calculations.

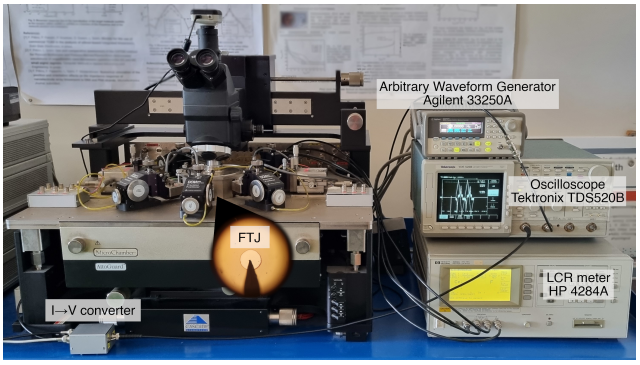

Figure 2: Picture of the experimental setup used for the FTJ characterization. The AWG Agilent 33250A drives the FTJ top electrode, while the output of the I→V converter is measured during time by the oscilloscope Tektronix TDS520B (see Fig. 1). FTJs under test are circular capacitors (see the central spot) with a diameter ranging from 110 μm to 450 μm and they are measured directly on wafers through the Cascade probe station. The setup includes also the HP4284A LCR meter for the measurement of the FTJ differential capacitance.

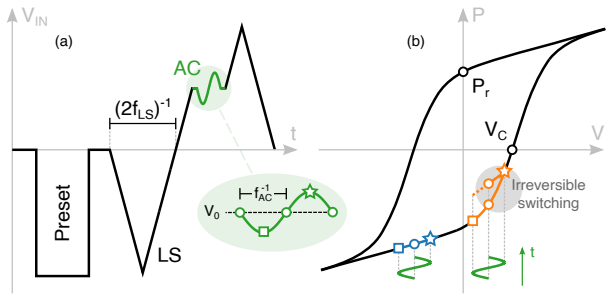

Figure 4: (a) Sketch of the AC measurement performed with the in–house–developed setup. To mimic the LCR meter measurement, the large signal (LS) voltage is swept accordingly to the reported triangular pulse. A sinusoidal (or triangular) AC signal is issued at a given V_0 bias. (b) Sketch of the P–V paths followed by the FTJs undergoing the AC signal, when V_0 is in the linear (blue) or switching branch (orange) of the P–V hysteresis. V_c is the positive coercive voltage of the FTJ.

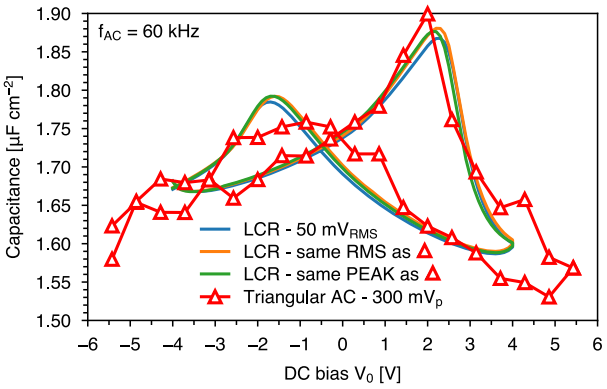

Figure 6: Small–signal capacitance either calculated from the amplitude of the I_{FTJ} measured with the setup issuing 60 kHz / 300 mV triangular waves (red triangles) or measured through the LCR meter issuing 60 kHz sinusoidal waves. LCR meter measurements are shown for a 50 mV RMS amplitude (blue), and for the same RMS (orange) and the same peak amplitude (green) as the triangular pulses.

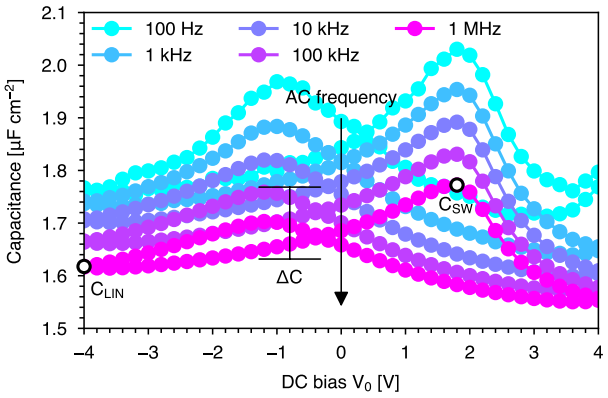

Figure 7: Differential capacitance versus voltage curves measured with the LCR meter in the 100 Hz — 1 MHz range. In the figure, the difference ΔC between the capacitance peak C_{SW} and the baseline C_{LIN} is highlighted.

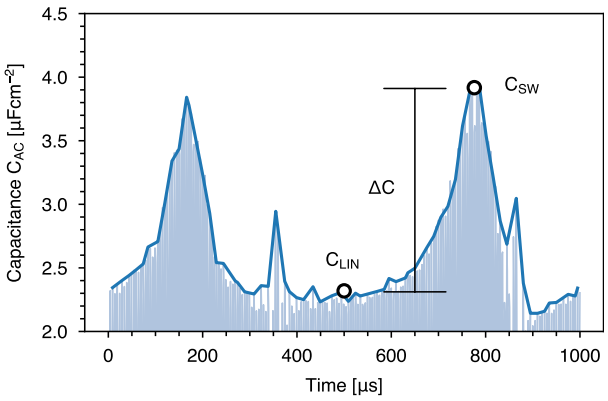

Figure 9: AC capacitance obtained from the high–frequency component of the experimental I_{FTJ} in Fig.8(b). This component is obtained by numerically high–pass filtering. The capacitance is calculated from the AC filtered current I_{AC} as $C_{AC} = I_{AC} \times (dV/dt)^{-1}$. The linear capacitance C_{LIN}, the capacitance at the switching peak C_{SW} and the difference $\Delta C = C_{SW} - C_{LIN}$ are highlighted.

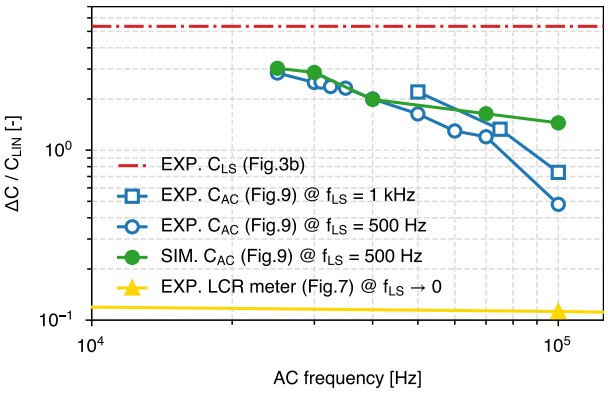

Figure 11: Relative difference between C_{SW} and C_{LIN} obtained from Fig.9 while sweeping f_{AC} (see Fig.8a) and for two LS triangular wave frequencies (blue). The values obtained from the LCR meter (yellow) and from C_{LS} in Fig.3b (red dot–dashed) are also reported as a reference. C_{SW} increases while reducing f_{AC}. Such behavior is not observed in the standard LCR meter experiments. Simulation results (green) agree quite well with the experimental trend.

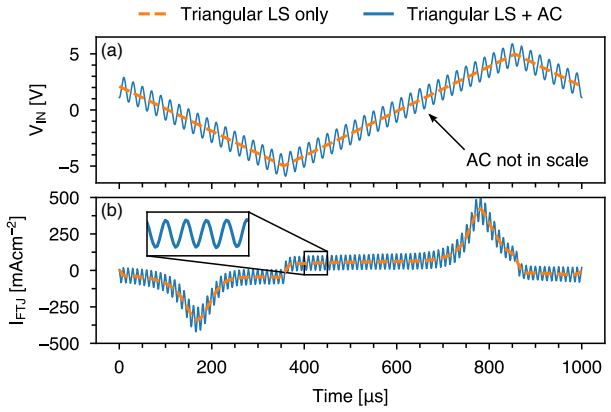

Figure 8: (a) Input signal (blue) for the novel AC analysis obtained as the superimposition of a slow triangular pulse (dashed orange, 1 kHz) and a sinusoidal waveform (f_{AC} = 100 kHz, 50 mV peak amplitude). (b) Measured I_{FTJ} (blue) shows 100 kHz sinusoidal fluctuations superimposed to the component due to the slowly varying triangular pulse (dashed orange).

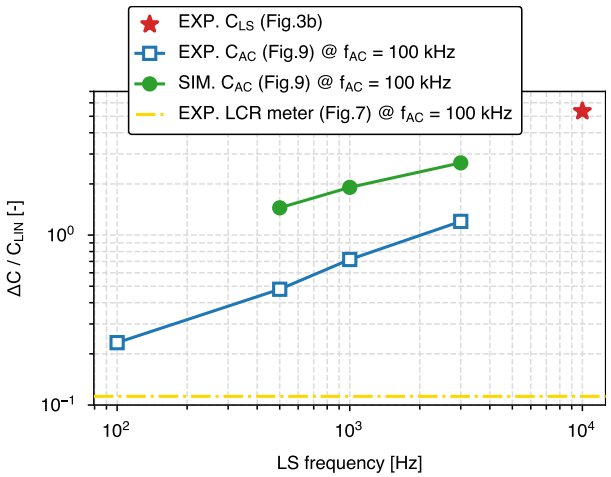

Figure 10: Relative difference between C_{SW} and C_{LIN} (blue) obtained from Fig.9 while sweeping the frequency of the LS triangular wave in Fig.8a and for a fixed f_{AC} = 100 kHz. The values obtained from the LCR meter experiments (dashed yellow line) and from C_{LS} in Fig.3b (red star) are also reported as a reference. C_{SW} increases while increasing the speed of the LS triangular wave. Simulation results (green) qualitatively reproduce the experimental trend.

[1] S. Slesazeck et al., *Nanotechnology*, vol. 35, p. 352003, 2019.

[2] R. Fontanini et al., *IEEE TED*, vol. 69, pp. 3694–3699, 2022.

[3] R. Fontanini et al., *IEEE JEDS*, vol. 9, pp. 1202–1209, 2021.

[4] S. Deng et al., *IEDM Tech. Digest*, p. 4.4.1, 2020.

[5] K. Toprasertpong et al., *IEDM Tech. Digest*, p. 23.7.1, 2019.

[6] J. Li et al., *IEEE Symposium on VLSI Technology*, p. 1, 2020.

[7] Y. Qu et al., *IEEE TED*, vol. 67, pp. 5315–5321, 2020.

[8] M. Massarotto et al., *SSE*, vol. 194, p. 108364, 2022.

[9] T. Rollo et al., *Nanoscale*, vol. 12, pp. 6121–6129, 2020.

[10] M. Segatto et al., *IEEE JEDS*, vol. 10, pp. 324–333, 2022.

Acknowledgments. This work is funded by the European Union through the BeFerroSynaptic Project (GA: 871737).